Parallel Compliance Design for Increasing Robustness and Efficiency in Legged Locomotion—Proof of Concept

Maziar Ahmad Sharbafi, Mohammad Javad Yazdanpanah, Majid Nili Ahmadabadi, and Andre Seyfarth

***Abstract*—Benefiting from serial compliance in series elastic actuators can be considered as a breakthrough in robotics. Recently, applying the parallel compliance in robot designs is growing based on its advantages such as reduction in consumed torques. In this paper, we aim at employing parallel compliance to increase walking robustness of bipedal robots against model uncertainties. Utilizing passive compliant elements instead of adapting the controller in order to cope with uncertainties makes the system more efficient and less sensitive to measurement issues such as delays and noise. We introduce a methodology for designing both parallel compliance and controller using hybrid zero dynamics concept. This study includes simulation results representing the design approach and preliminary experiments on parallel compliance effects on efficiency of a robot joint position control. The simulations comprise a compass gait (2-link) model and a 5-link model. The ground slope and robot segment lengths are considered as uncertain parameters in the first and second models, respectively. The control target is met by the insertion of compliant structures parallel to the actuators. In order to employ the proposed method on a real robot, we suggest using pneumatic air muscles as parallel compliant elements. Pilot experiments on the knee joint of BioBiped3 robot support the feasibility of suggested method.**

***Index Terms*—Hybrid zero dynamics, legged locomotion, nonlinear control systems, robustness.**

Manuscript received April 28, 2018; revised April 30, 2019; accepted May 9, 2019. Date of publication May 16, 2019; date of current version August 14, 2019. Recommended by Technical Editor Q. Wang. This work was supported by the German Research Foundation (DFG) under Grant AH307/2-1 and Grant SE1042/29-1. *(Corresponding author: Maziar Ahmad Sharbafi.)*

M. A. Sharbafi is with the Control and Intelligent Processing Center of Excellence (CIPCE), School of Electrical and Computer Engineering, University of Tehran, Tehran 14395-515, Iran, and also with Lauflabor Locomotion Laboratory, Institute of Sport Science, Centre for Cognitive Science, TU Darmstadt, 64283 Darmstadt, Germany (e-mail: sharbafi@ut.ac.ir).

M. J. Yazdanpanah and M. N. Ahmadabadi are with the Control and Intelligent Processing Center of Excellence (CIPCE), School of Electrical and Computer Engineering, University of Tehran, Tehran 14395-515, Iran (e-mail: yazdan@ut.ac.ir; mnili@ut.ac.ir).

A. Seyfarth is with Lauflabor Locomotion Laboratory, Institute of Sport Science, Centre for Cognitive Science, TU Darmstadt, 64283 Darmstadt, Germany (e-mail: seyfarth@sport.tu-darmstadt.de).

Color versions of one or more of the figures in this paper are available online at http://ieeexplore.ieee.org.

Digital Object Identifier 10.1109/TMECH.2019.2917416

I. Introduction

SERIES elastic actuators (SEAs, [1]) provide clear benefits for artificial legged locomotor systems by adding compliance to the traditional rigid actuators [e.g., electric motors (EM)] [2]–[4]. In comparison with non-compliant actuators, the SEA has lower impedance, higher efficiency, and robustness against perturbations [5], [6]. These advantages are obtained by restoring energy through serial elasticity of the actuator. This behavior mimics the stretch-shortening cycles in biological muscle, [7]. Furthermore, Hurst showed that adding compliance to the robot structure considerably simplifies control [8]. One step further will be stiffness adjustment in variable impedance actuators (VIAs) [9] which is mainly attained by addition of a second actuator for adapting to different gait conditions (e.g., speed). Although the VIA improves the controllability of the output which is useful for enabling legged robots to cope with uncertainties and perturbations, the mechanical design and control are much more complex [9], [10] than EM and SEA. In addition, both actuators in a VIA continuously produce torques during the movement (e.g., as in the humanoid robot Veronica [10]), and hence it can reduce the required power, but not the torque [11], [12].

The addition of a parallel compliant element to an actuator can reduce EM torque, as the joint torque does only partially pass through the motor [6], [11]. Auxiliary parallel compliance (PC) can help to achieve the required torques above the actuator limitations. By adding such parallel compliant elements, the control efforts shift to stabilizing the motion [12]. With added PC and matching control effort, system stability and robustness against uncertainties can be improved [11]. It is also in line with muscular parallel passive compliance (epimysium and titin [13]) in biological locomotor systems [14]. In [15], the advantages of appropriate mechanical design to enhance control were shown and compared with findings in human walking. In studies on mimicking human ankle joint behavior with a prosthetic foot, Grimmer *et al.* showed that the required peak power and peak torque can be reduced by adding a PC [16]. With a well-designed biped having humanlike body characteristics (e.g., compliant muscles), a simple open-loop controller can stabilize walking [17], [18].

In [19], using the concept of virtual constraint (VC), the controller was designed with feedback linearization and

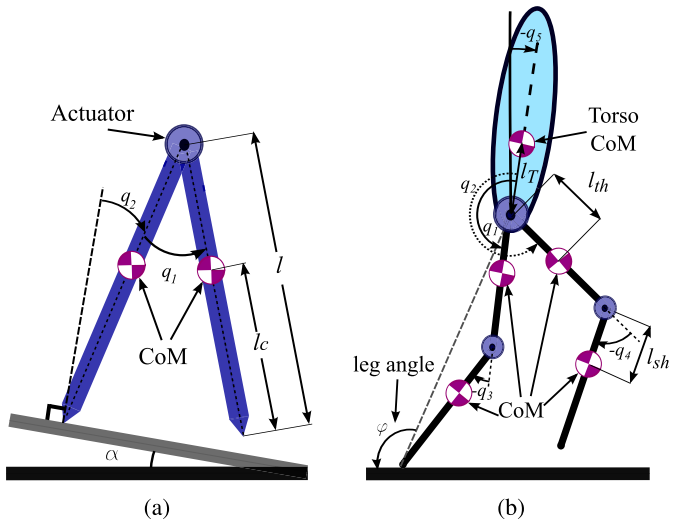

Fig. 1. Schematic and definitions of variables and parameters in (a) Acrobot model and (b) 5-link model.

the hybrid zero dynamics (HZD) method was introduced for stability analyses. Later, the compliance (as a physical constraint) was inserted to the robot joints to increase the control efficiency and the stability was investigated using HZD concept [20], [21]. Hence, both physical and virtual adjustable impedance could be employed for design and control [8], [19], [22]. Inspired from the compliant HZD control approach, here, we introduce a method to shape motion dynamics via deliberate insertion of passive compliant elements, parallel to the robot's actuators. With that, we can simultaneously design and control a robust and efficient locomotor system.

This paper is organized as follows: Section II presents the basic concepts of modeling and the HZD control from [19]. In Section III, the proposed method including an algorithm to design HZD-based compliant controller is explained. The supporting theorems are presented here, but some of the proofs are described in a complementing paper [23]. Section IV comprises two simulation and one experimental results. Robustness against uncertainties in the ground slope and body parameters are targeted by simulation models (see Fig. 1). The results of a pilot study on employing pneumatic artificial muscle (PAM), as adjustable compliance, are described at the end of this section. Discussions and future steps are presented in Section V.

II. Basic Concepts

Here, we describe the HZD control method after presenting a short overview of the modeling approach.

A. Dynamic Model

We consider an $N-link$ model with point feet and without any closed chain as introduced in [19]. A hybrid model is utilized for such a system including continuous and discrete subphases. The single support phase, which defines the continuous part, consists of ordinary differential equations describing the motion of the robot when only one leg is in contact with the ground and the other leg swings forward. In the double support phase, a discrete subsystem models the impact when the swing leg touches the ground. Let the system states $q=[q_1,\ldots,q_N]^T$, in which the first $N-1$ variables are the joint angles and the last one (q_N) is the angle between the unactuated foot contact and the ground. Two samples are shown in Fig. 1. Since the HZD controller can be applied to models with higher degrees of underactuation [15], [24], this is also valid for our control approach.

From Largrange equation, the swing phase dynamics is determined as follows:

$$\dot{x}=\begin{bmatrix}\dot{q}\\ D^{-1}(q)[-C(q,\dot{q})\dot{q}-G(q)+Bu]\end{bmatrix}=f(x)+g(x)u \tag{1}$$

in which D, C, G, and B are the inertia, Coriolis matrices, the gravity vector, and a constant matrix that maps the joint torque vector u to the generalized forces, respectively. In addition, the state variables are defined by $x=[q,\dot{q}]^T$. When the swing leg hits the ground, an inelastic impact Δ occurs. The hybrid walking model will be

$$\Sigma=\begin{cases}\dot{x}=f(x)+g(x)u & x^-\notin\mathcal{S}\\ x^+=\Delta(x^-) & x^-\in\mathcal{S}\end{cases} \tag{2}$$

in which $\mathcal{S}$ is the switching surface and super-indexes $^-$ and $^+$ denote the moments exactly before and after impact, respectively.

B. Designing HZD Controller

Our control approach is utilizing HZD [25], [26] to design virtual and physical constraints. The holonomic constraints on the robot's configuration, which are asymptotically achieved through the feedback control action, are defined as virtual constraints, $y=h(q)$ [27]. This virtual constraint approach has been very successfully applied in designing feedback controllers for planar bipedal robot walking with stability proof [25], [27], [28]. In HZD control design, the control torque is determined via feedback linearization to regulate the output (y) to zero which provides a stable attractive manifold, namely "HZD manifold"

$$u(x)=(L_gL_fh(x))^{-1}(\overbrace{-K_D\dot{y}-K_Py}^{v}-L_f^2h(x)) \tag{3}$$

where $L_fh(x):=\frac{\partial h}{\partial x}f$ is the Lie derivative[1] of h along f and repeating this operator on $L_fh(x)$ along g and f, results in $L_gL_fh(x)$ and $L_f^2h(x)$, respectively. We assume L_gL_fh is invertible. With regulation of the output to zero, the investigation of the internal stability which is performed by analyzing the internal dynamics, reduces to the zero dynamics [30]. Here, we use a PD controller [v in (3)] to obtain input–output stability. Let $\eta:=[h(q);L_fh(q)]$; using a diffeomorphism transform T, the normal form can be computed with new variables

[1]See [29] for description about feedback linearization and definitions, e.g., the Lie derivative.

$z := [\eta; \xi] = T(x)$ as

$$\dot{\eta} = \begin{bmatrix} 0 & I \\ 0 & 0 \end{bmatrix} \eta + \begin{bmatrix} 0 \\ I \end{bmatrix} (L_g L_f h(x) u + L_f^2 h(x))$$
$$\dot{\xi} = f_i(\eta, \xi), \tag{4}$$

in which, x will be replaced by $T^{-1}(z)$ and $f_i(\eta, \xi)$ describes the internal dynamics. On the zero dynamics manifold $\mathcal{Z} := \{z | \eta = 0\}$, the internal dynamics [the second subsystem in (4)] is simplified to the zero dynamics $\dot{\xi} = f_0(\xi)$ where $f_0(\xi) := f_i(0, \xi)$ (see [19] for details).

Definition 1. Hybrid zero dynamics: Consider the hybrid model (2) and $\dot{\xi} = f_0(\xi)$ for the zero dynamics of the swing mode, if zero dynamics manifold $\mathcal{Z}$ is hybrid invariant, meaning

$$\Delta(\mathcal{S} \cap \mathcal{Z}) \subset \mathcal{Z} \tag{5}$$

then the HZD of (2) is given by

$$\Sigma_0 := \begin{cases} \dot{\xi} = f_0(\xi), & \xi^- \notin \mathcal{S} \cap \mathcal{Z} \\ \xi^+ = \Delta(\xi^-) & \xi^- \in \mathcal{S} \cap \mathcal{Z} \end{cases} \tag{6}$$

Satisfying the hybrid invariance condition (5), the stability of the HZD as a low dimensional system (related to the degree of underactuation) results in stability of the full model [25]. Computing the normal form and evaluating it on $\mathcal{Z}$, results in zero dynamics equations. To analyze the stability of HZD, contact with Poincaré section, which results in Poincaré map, is utilized [19]. With this technique, the stability analysis is restricted to the investigation of the one-dimensional discrete system, generated by the Poincaré map. For this, the states of zero dynamics can be written as $\xi = [\xi_1, \xi_2]^T$. Then, the zero dynamics will be given by

$$\begin{cases} \dot{\xi}_1 = \kappa_1(\xi_1)\xi_2 \\ \dot{\xi}_2 = -\kappa_2(\xi_1) \end{cases} \tag{7}$$

As suggested in [19], we define new variables $[\zeta_1, \zeta_2] = [\xi_1, \xi_2^2/2]$ which summarizes the zero dynamics stability analysis to the stability of the discrete map $\rho(.)$ presented by

$$\rho(\zeta_2^-) = \delta_{\text{zero}} \zeta_2^- + V_{\text{zero}}(q_2^-). \tag{8}$$

This Poincaré map finds the new variable (ζ_2^-) at preimpact moment of each step, from its previous value. In this equation, δ_{zero} is a positive value that demonstrates the impact effect for the new state variable $(\zeta_2^- = \delta_{\text{zero}} \zeta_2^+)$ and $V_{\text{zero}}(q_2)$ is calculated by integrating $\frac{d\zeta_2}{d\xi_1}$ from postimpact leg angle to q_2 as follows:

$$V_{\text{zero}}(q_2) = \int_{q_2^+}^{q_2} \frac{\kappa_2(q)}{\kappa_1(q)} dq. \tag{9}$$

Assume $V_{\text{Zero}}^{\text{Max}} = \max_{q_2^+ \le q_2 \le q_2^-} V_{\text{zero}}(q_2^-)$; if the following condition is satisfied:

$$C_1 \equiv \zeta_2^+ - V_{\text{zero}}^{\text{Max}} > 0 \tag{10}$$

then ζ_2^- can be calculated by

$$\zeta_2^- = \zeta_2^+ - V_{\text{zero}}(q_2^-). \tag{11}$$

Analyzing slippage equations during the swing phase and at impact besides the above discussions summarizes the stability conditions in periodic walking with HZD controller in the next theorem (see [19] for proofs).

Theorem 1: Consider the model presented by (2) satisfying conditions (5) and (10), then the bipedal walker with HZD controller defined by (3) has a stable periodic motion, if and only if all the following conditions are satisfied:

$$0 < \delta_{\text{zero}} < 1 \tag{12}$$

$$C_2 \equiv \frac{\delta_{\text{zero}}}{1 - \delta_{\text{zero}}} V_{\text{zero}}(q_2^-) + V_{\text{Zero}}^{\text{Max}} < 0 \tag{13}$$

$$C_3 \equiv \delta_{\text{zero}} \zeta_2^- - V_{\text{Zero}}^{\text{Max}} > 0, \tag{14}$$

$$\frac{F^T}{F^N} > \mu_s, \qquad F^N > 0. \tag{15}$$

□

In condition (15) which prevents slipping, μ_s, F^T, and F^N are the friction coefficient, the tangential, and normal forces at the foot contact with the ground, respectively. Violating (14) means that the robot does not spend enough energy to finish a step successfully [19]. Our theoretical description of the proposed method (presented in the following sections) is based on this theorem.

The final step in designing the controller is determining the virtual constraints. For this, we formulate the output as the difference between the targeted variable (e.g., q_1 in Acrobot model) and the desired function (h_d) of the guiding variable (q_2 in Acrobot). Then, defining virtual constraints is restricted to the design of $h_d(q)$. The Bézier polynomial is commonly used to approximate the virtual constraints [22], [25], [31]. In Acrobot with only one actuator, the output can be defined with a holonomic constraint $y = h(q) = q_1 - h_d(q_2)$ and the quadratic polynomial is sufficient for defining h_d. To meet the condition presented in (5), two coefficients of this polynomial are computed. From the hybrid invariance condition (5), the quadratic polynomial for virtual constraint will have the following formalism:

$$h_d(q_2) = \alpha_1 q_2^2 + 2q_2 - \alpha_1 {q_2^+}^2. \tag{16}$$

The remaining parameter α_1 is used to satisfy the stability conditions in Theorem 1. As described earlier, after satisfying the stability conditions resulted from Poincaré map analysis, there are still parameters to be selected mostly by optimization approaches. We select the integral of the squared consumed torque $u(t)$, divided by the traveled distance (d) in one step period (T) to minimize energy consumption

$$J = \frac{1}{d} \int_{t_0}^{t_0+T} \|u(t)\|^2 dt \tag{17}$$

III. Designing a Compliant HZD Controller

In this section, the design of the controller and determining the proper PC are explained as a single problem. In [19], reconfigurability of the controller is mentioned as the most significant preference of the virtual constraints rather than the

physical ones. Furthermore, insertion of the compliance as a physical constraint adds many useful advantages in motion performance such as increasing robustness, reducing energy consumption, and fast recovery after disturbances [8], [32]–[35].

We exploit the benefits of both methods by designing the controller based on virtual constraints and changing model dynamics with entering different types of compliance in the joint. In the design of our *HZD+parallel compliance (HPC) controller* (see Section III-D), the model without uncertainty is called *nominal model*.

A. Uncertainties and Robustness Range

In order to explain the design steps of the HPC controller, we introduce *uncertainty* and *robustness range*.

Definition 2: Uncertainty range $\mathcal{P}$ is defined as the range for the uncertain parameter values p to cope with (e.g., downhill ground slope upto 10° gives $\mathcal{P} = [0\ 10]$). This range is defined such that for every parameter set $p \in \mathcal{P}$, there exists at least one HZD controller that results in stable walking. All controllers must have the same virtual constraints [the function of $h(q)$)]. For a parameter set $p \in \mathcal{P}$, subindex p is utilized to show the related functions, matrices, and vectors (e.g., D_p for inertia matrix using parameter set p).

Definition 3. Norm, distance and neighborhood: The norm used in this paper is "2-norm." The distance of two vectors v_1 and v_2 is defined by $||v_1 - v_2||$. Distance to a manifold for a point $p \in \Re^n$ to a manifold $\mathcal{M} \in \Re^n$ is $|p|_{\mathcal{M}} = \inf_{m \in \mathcal{M}} \{||m - p||\}$. For a manifold $\mathcal{M} \in \Re^n$ and positive constant ϵ, subset $\mathcal{N}(\mathcal{M}, \epsilon) = \{p \in \Re^n \mid |p|_{\mathcal{M}} \leq \epsilon\}$ is called the ϵ-neighborhood of manifold $\mathcal{M}$.

Consider the normal form (4) with addition of model uncertainty in which the real model is different from the nominal model. It is shown that after feedback linearization with controller (3), the system will have *matched uncertainty*[2] [29], [30]; $\delta(z)$, as follows:

$$\dot{\eta} = \overbrace{\begin{bmatrix} 0 & I \\ -K_P & -K_D \end{bmatrix}}^{A_c} \eta + \overbrace{\begin{bmatrix} 0 \\ I \end{bmatrix}}^{b} \delta(z)$$
$$\dot{\xi} = f_i(\eta, \xi). \tag{18}$$

Lemma 1: Consider system (18), where A_c is Hurwitz and ξ^* is the zero-invariant set[3] of the internal dynamics $\dot{\xi} = f_i(\eta, \xi)$. Suppose that ξ^* is the asymptotically stable manifold of the zero dynamics and the uncertainty $\delta(z)$ satisfies

$$||\delta(z)|| \leq \gamma ||\eta|| + \epsilon \tag{19}$$

for nonnegative constants γ and ϵ. For every $\epsilon_M > 0$, a neighborhood $\mathcal{D}$ around $z^* = [0; \xi^*]$, matrices K_P and K_D, and time t_0 can be found such that

$$|z(t)|_{z^*} \leq \epsilon_M, \forall t \geq t_0, \forall z(0) \in \mathcal{D}. \tag{20}$$

□

[2]The uncertain terms enter the state equation at the same point as the control input.

[3]A zero-invariant set $\mathcal{A}$ for a system $\dot{x} = f(x, u)$ is an invariant set of the unforced system $\dot{x} = f(x, 0)$, meaning $x_0 \in \mathcal{A} \Rightarrow x(t, x_0, 0) \in \mathcal{A}$, $\forall t > 0$.

The derivation of (18) and the proof of Lemma 1 are described in [23]. This lemma is presented for the continuous system (18) and we extend it to hybrid systems in the following section. We assume that the uncertainty δ is bounded which is a reasonable requirement that follows from continuous differentiability of the nonlinear functions [29]. This upperbound does not have a direct relation to ξ. This means that the influence of ξ (and higher orders of η) on the uncertainty are considered in ϵ.

Definition 4: In a bipedal walking model stabilized by HZD controller (3), the *robustness range* is defined by (ϵ^*, γ^*) for which the matched uncertainties $||\delta|| \leq \gamma^* ||\eta|| + \epsilon^*$ cannot destabilize the controlled system.

Definition 5: Maximum impact of uncertainty on HZD is defined by the infinite norm of the decoupling matrix for the uncertain system on the zero dynamics manifold as follows:

$$U_p = \sup_q ||\frac{\partial h}{\partial q} D_p^{-1} B|_{\mathcal{Z}}||. \tag{21}$$

In addition, we find *the uncertainty bias upper limit* by the following equation:

$$U_m = \sup_{p \in \mathcal{P}} U_p. \tag{22}$$

This relation means that the bias term of uncertainty [ϵ in (19)] has an upper limit. In other words, the growth of the matched uncertainty is not faster than a linear function of η.

B. Increasing Robustness With PC

In this section, it is shown that the addition of appropriate compliance parallel to the actuators could preserve stability in a wide range of parameter variations. Accordingly, a design methodology will be presented in the next section. For modeling an additional torque vector $[\tau_c(q, \dot{q})]$ that is produced by the joint compliance (parallel to the actuators), u in (1) should be replaced by $u + \tau_c$.

Definition 6: For the two matrices K_P and K_D with largest singular values $\bar{K}_P$ and $\bar{K}_D$, respectively, we define the control gain K_{PD} as follows:

$$K_{PD} := \frac{\bar{K}_P \bar{K}_D}{\bar{K}_P + \bar{K}_D}. \tag{23}$$

Theorem 2: Consider the bipedal walker dynamic model (2) with the nominal parameter set $n \in \mathcal{P}$ (called Σ_n) and HZD controller K_n (producing control torque u_n). Suppose that for a parameter set $p \in \mathcal{P}$ different from n, a controller (K_p with control torque u_p) using virtual constraints [$h(x)$], and PD coefficients (K_P and K_D) equal to those of the nominal model, generates stable walking for the uncertain system Σ_p.

If there exists positive ϵ^* such that

$$||u_n - u_p|| \leq \frac{\epsilon^*}{||U_p||} \tag{24}$$

and

$$K_{PD} \geq 2\Pi_m(q)||u_n - u_p|| \tag{25}$$

in which K_{PD} is given by (23) and $\Pi_m(q)$ is the supremum of the distance between $L_g L_f h(q)_p$ and its projection on the zero

dynamics manifold $\mathcal{Z}$, divided by the output $h(q)$. Then, the HZD controller K_n stabilizes Σ_p. □

Theorem 3: Consider the two systems (Σ_n and Σ_p) with parameter sets n and p, satisfying conditions of *Theorem 2*, except (24). Suppose that a set of compliant elements produces the additive torque vector τ_c parallel to the actuator torque vector (u). If

$$\begin{cases} ||\tau_c|| \leq \min\left(\frac{K_{PD}}{2\Pi_n}, \frac{\epsilon^*}{U_n}\right) \\ ||u_n + \tau_c - u_p|| \leq \min\left(\frac{K_{PD}}{2\Pi_p}, \frac{\epsilon^*}{U_p}\right) \end{cases} \tag{26}$$

then, the HPC controller K_c—comprises K_n and compliance τ_c—stabilizes both systems Σ_n and Σ_p. □

The proofs of the theorems are presented in the complementary paper [23]. The importance of Theorem 3 is in presenting a new controller which can stabilize both systems Σ_n and Σ_p without knowing the correct parameters. When condition (24) is not satisfied, the nominal controller K_n cannot stabilize the system with uncertain parameter p, meaning that this controlled system is not robust against such an uncertainty. By adding the PC τ_c to the actuator, deviation from nominal controller is accepted in order to increase robustness. Therefore, the HPC controller will have lower performance in the nominal case and higher robustness against uncertainties. As a result, PC can increase the robustness range up to its double size (proved in Section III-C).

C. Robust HZD-Based Controller Design

In this section, we present a method to design an HZD-based controller and in the next section we explain how to insert PC to increase robustness passively. Instead of an attractive manifold, we introduce an attractive region for satisfying boundedness in a range of parameters. Here, first we design a nominal controller K_n for all $N-1$ active joints using virtual constraints that work for any $p \in \mathcal{P}$. Then, for each joint we modify the controller to increase the robustness as follows.

i) Find extremes of actuation with respect to parameter p

$u_{\min}(q,\dot{q}) = \inf_p u_p(q,\dot{q})$, and $u_{\max}(q,\dot{q}) = \sup_p u_p(q,\dot{q})$.

ii) Define the robust HZD-based controller K_r with the following control effort:

$$u_r(q,\dot{q}) = \frac{u_{\max}(q,\dot{q}) + u_{\min}(q,\dot{q})}{2}. \tag{27}$$

Suppose that a controller K_c generates actuation $u_c(q,\dot{q})$. For a specific set of parameters p, let us define the maximum difference between the desired HZD controller u_p and u_c by $\delta u_c^p = \sup_{q,\dot{q}} ||u_c - u_p||$. This difference shows the maximum torque to be added to controller u_c that gives the required torque u_p. The lower this difference, the less required additional torque which means that controller u_c is less different than the desired one and is more robust against uncertainties. Among the whole parameter range, the largest difference between the controller u_c and the desired HZD controllers in full information case (u_p) can be found as $\overline{\delta u_c} = \sup_p(\delta u_c^p)$.

Let us define

$$du(q,\dot{q}) = \frac{u_{\max}(q,\dot{q}) - u_{\min}(q,\dot{q})}{2}. \tag{28}$$

From the definition of our robust HZD controller K_r in step (ii), we have

$$\overline{\delta u_r} = \sup_p(\delta u_r^p) = \sup_{q,\dot{q}} du(q,\dot{q}). \tag{29}$$

Therefore, the robustness range of a nominal controller u_n can be increased up to double size as shown in the following:

$$\overline{\delta u_r} \leq \overline{\delta u_n} \leq 2\overline{\delta u_r}. \tag{30}$$

This equation shows that compared to a nominal model u_n, the norm of the difference between the produced toque and desired torque $\overline{\delta u_n}$ is larger than that of the robust controller $\overline{\delta u_r}$. The ratio between these two numbers could increase up to 2, which means the controller u_r could be two times more robust than u_n against parameter uncertainties.

Theorem 4: Assume there is no nominal controller K_n satisfying condition (24) for all uncertain parameter $p \in \mathcal{P}$. The controller K_r given by (27) is robust against uncertainty p, if the following condition is held:

$$||u_{max} - u_{min}|| \leq \min\left(\frac{K_{PD}}{\Pi_m}, \frac{2\epsilon^*}{U_m}\right). \tag{31}$$

□

The proof is presented in [23]. Condition (31) satisfies (24) for any uncertain parameter $p \in \mathcal{P}$ if and only if the controller is the robust HZD controller K_r. For example, if the "$\leq$" turns to "$=$", the controlled system for any HZD controller except K_r is not robust against uncertainties in the whole region. It is noticeable that the proposed robust controller K_r is not a standard HZD controller, and then there is no closed form control formulation for u_r. In addition, this controller needs to compute the required torque for the uncertain parameter changing in the whole uncertain region at each instants of time, which is computationally expensive. To resolve these issues, we propose a method to design a hybrid compliant controller to benefit from advantages of producing part of the control effort by parallel passive elements.

D. Robust HPC Controller Design

In this framework the PC and the controller (HZD) are simultaneously designed resulting in a hybrid controller with mixture of virtual and physical constraints. The compliant elements are considered in the $N-1$ active joints. We consider a (nonlinear) function [$\tau_c(q,\dot{q})$; e.g., a polynomial] of the joint angle (q) and angular velocity ($\dot{q}$). No constraint in defining compliance function $\tau_c(q,\dot{q})$ is enforced by the HPC control design method. Therefore, any implementable impedance function can be used for $\tau_c(q,\dot{q})$. One step further is to design new functions which can increase robustness and then to find methods for the physical implementation. Later, we introduce one solution which is employing the PAM as an adjustable PC. We have identified the dynamic model of PAMs [36], which can be used as nonlinear function τ_c (tunable by the injected amount of air) to design the hybrid controller.

Definition 7: We assume that the walking model is controllable with a parameter-dependent HZD controller K_p, if the uncertain parameter $p \in \mathcal{P}$ is known. In such a condition,

a fixed virtual constraint which is used for the controller with full information (known p) is called *stabilizing VC*.

The goal is to design an HPC controller to work in the whole range of uncertain parameters $p \in \mathcal{P}$. Based on Theorem 4, there is no standard HZD controller that is robust against every p (as an uncertain parameter) in the whole region $\mathcal{P}$. The algorithm that gives the desired compliance for each joint, includes two main parts:

Part 1: Defining the nominal model

1) Consider a set of parameters as the nominal model Σ_n.
2) Design an HZD-based controller K_n for the nominal model Σ_n with (3) using the *stabilizing VC* (working for any $p \in \mathcal{P}$).
3) Find $u_{min}(q,\dot{q}) = \inf_p u_p(q,\dot{q})$ and $du_p = u_p(q,\dot{q}) - u_{min}(q,\dot{q})$.
4) Find $n_{min} = \text{argmin}_p\{\sup_{q,\dot{q}} du_p(q,\dot{q})\}$.
5) If $\Sigma_n = \Sigma_{n_{min}}$ continue, otherwise set $\Sigma_n = \Sigma_{n_{min}}$ and jump to step 2.
6) Define u_{min}, u_{max}, and the robust HZD controller K_r (27), from steps (i) and (ii) in Section III-C.

Here, u_{min} and u_{max} define the variation range of the control inputs in this region of parameter changes. As aforementioned, there is no HZD controller that stabilizes the system for every uncertain parameter set $p \in \mathcal{P}$ while parameter p is not known.[4] In this method, searching in the uncertain range to find extreme values is applied offline and the computational cost is not important. Based on these two parts, finally, we introduce one HZD controller that is given with an analytical formulation plus PC and the computational cost of the proposed mixed controller is not higher than that of an HZD controller.

Part 2: Designing the compliance and control modification

1) Let $\delta u(q,\dot{q}) = u_r(q,\dot{q}) - u_n(q,\dot{q})$ and find the parameters of the compliant structure $\tau_c(q,\dot{q})$ to minimize $\delta\tau := \sup_{q,\dot{q}} ||\delta u - \tau_c||$.
2) Using $\overline{\delta u_r}$ from (29), let $R := \overline{\delta u_r} + \delta\tau$ and K_{PD} from Definition 6; if $K_{PD} < 2\Pi_m R$, multiply PD gains by $\frac{2\Pi_m R}{K_{PD}}$ and go to Step 2 of part 1.
3) For the nominal model, find the upper bound ϵ^* of the robustness range, based on Definition 4.
4) Compute $\epsilon = RU_m$; if $\epsilon > \epsilon^*$ change the compliance structure and go to Step 1.
5) The HPC controller K_c is defined by the controller K_n plus the compliance τ_c.

Theorem 5: The HPC controller produces a stable closed-loop system for the whole uncertain region $\mathcal{P}$.

The proof of this theorem, which is based on Theorems 2–4, is presented in [23]. The proposed algorithm provides an instruction to design a robust controller comprising an HZD controller and a PC, which is called HPC controller. In the following we describe how to use this method in two different case studies.

[4]The controller and the virtual constraints are designed such that K_p can control the system in the whole uncertain region $\mathcal{P}$ if the parameter set p is known.

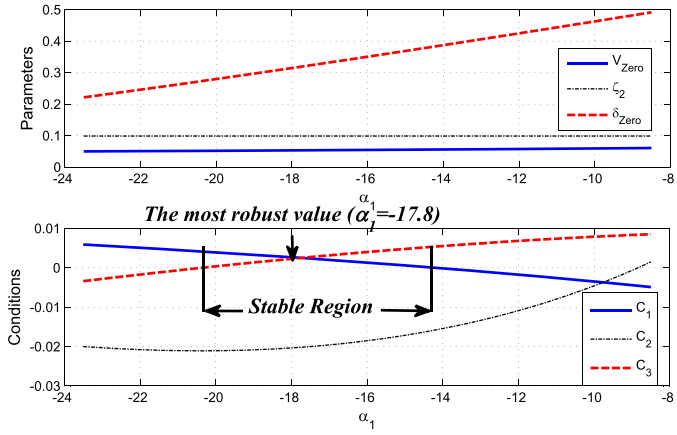

Fig. 2. Controlled system specifications according to coefficient variation. (Top) Parameters which are needed to show the stability. (Bottom) Conditions which should be checked.

E. Case Study 1: Acrobot Model

The first case is developing a robust controller for walking with the Acrobot model on an unknown slope (uncertain parameter p). In this model, there is one place to add PC to the actuator at hip joint and the extremes (u_{max} and u_{min}) can be analytically computed as a function of the ground slope. Here, we describe the details of designing the HPC controller for the Acrobot model which is divided into two parts. First, the method of selecting the most robust HZD controller (without compliance) that can be obtained by changing the free parameter of the quadratic polynomial is described. Then, the effect of inserting compliant elements with different structures is explained. The superiority of nonlinear structure for increasing the robustness, which was introduced before in [37] and [38], is approved in Section IV. In control of the Acrobot model, the ground slope in the nominal model is set to zero (flat terrain) and different values for the slope are considered as the uncertainty to evaluate the robustness. The equations of motion are implemented within Matlab/Simulink applying the ode45 solver. The mechanical properties of the Acrobot are taken from [39].

1) Designing a Robust Controller for the Flat Surface: Analyzing the stability and robustness in this section is found in Theorem 1, in which conditions (5), (10), and (12)–(15) should be satisfied for stable walking. As stated before, in HZD controller with quadratic polynomial, if the virtual constraint has the form presented by (16), the first condition (5) is fulfilled. The upper and lower limits of α_1 are determined using the other stability conditions. Assume $q_2^+ = -13^\circ$, the variations of the necessary conditions with respect to α_1 are shown in Fig. 2. On the top figure, V_{Zero} and ζ_2 are positive and δ_{zero} is less than one for $-23.5 < \alpha_1 < -7.5$, which are necessary conditions for stability. Additional conditions for stability are satisfied if the blue (solid) and red (dashed) curves have positive, but the black (dotted) curve negative values in the bottom figure. Fig. 2 shows that only between -14.3 and -20.3 all the conditions are satisfied. This figure also depicts that the largest stability margin (the largest distance to zero) is achieved by $\alpha_1 = -17.8$.

TABLE I
FIVE-LINK MODEL PARAMETERS WITH HUMAN BODY CHARACTERISTICS [41]

Name	Parameter	value	unit
M_T	Torso mass	54	
M_{th}	Thigh mass	8	kg
M_{sh}	Shank mass	5	
L_T	Torso length	0.89	
L_{th}	Thigh length	0.5	m
L_{sh}	Shank length	0.5	
l_T	Hip to torso CoM distance	0.33	
l_{th}	Hip to thigh CoM distance	0.21	m
l_{sh}	Knee to shank CoM distance	0.3	
I_T	Torso inertia	10.6	
I_{th}	Thigh inertia	1.8	kgm^2
I_{sh}	Shank inertia	1	
g	Gravitational acceleration	9.81	m/s^2
μ	Static friction coefficient	0.6	–

2) Compliance Insertion: Different structures for compliance are investigated to find the most effective one for walking on the widest range of slopes. The compliant element is defined as $\tau_c = \tau_D + \tau_S$ including nonlinear (deadzone) characteristics for both spring (τ_S) and damper (τ_D) effects:

$$\tau_D = \begin{cases} 0 & \text{if } \dot{q}_1 \le d \\ B_d \dot{q}_1 & \text{otherwise} \end{cases} \tag{32}$$

$$\tau_S = \begin{cases} 0 & \text{if } q_1 \le s \\ K_s q_1 & \text{otherwise} \end{cases} \tag{33}$$

in which, B_d, K_s, d, and s are nonnegative constants and the spring rest angle is set to zero. Physical implementations of such mechanisms are possible, e.g., the seat belt is a sample of such a nonlinear damper. There is no restriction to define the nonlinear function except manufacturing feasibility.

F. Case Study 2: 5-Link Model

In the 5-link model, the upper body is represented by a rigid trunk and each leg has two segments for thigh and shank, as shown in Fig. 1(b). According to the angles demonstrated in the figure, the angle vector is defined by $q := [q_1 .. q_5]^T$. The leg angle $\varphi := \frac{3\pi}{2} - q_1 + \frac{q_3}{2} - q_5$ [shown in Fig. 1(b)], monotonically increasing during each step, can parameterize the virtual constraints. From results of human walking pattern in [40], it is observed that the joint angles can be characterized as functions of the leg angle. In that respect, we define the outputs as follows:

$$y_i = q_i - h_d^i(\varphi), \ i = 1, \ldots, 4 \tag{34}$$

in which $h_d^i(.)$s are polynomials of degrees smaller than 4. After satisfying the stability conditions, the polynomial coefficients are set to generate trajectories similar to the joint angles in human gaits [40]. By adopting the model parameters from human segment data [41] (see Table I) and with the HZD controller using virtual constraints (34), stable walking at different speeds (from 0.5 to 2.6 m s^{-1}) can be achieved [42]. Here we consider 1.2 m s^{-1} as moderate walking speed.

The model uncertainty is defined by considering $\pm 10\%$ deviation in the segments' lengths [$L = [L_T, L_{th}, L_{sh}]$, shown in Fig. 1(b)]. This type of uncertainty affects inertia matrix D, Coriolis matrix C, and gravity vector G. There is no HZD controller that can stabilize the motion with this uncertainty range and the mentioned virtual constraints. To solve this problem, an HPC controller is developed in which the compliance structure is constructed by rotational springs with linear force–angle relations.

G. BioBiped Experimental Setup

The BioBiped robot series is inspired by the muscular architecture of human leg (see http://www.biobiped.de/index/ and [4]). In this robot series, human muscles are modeled by passive springs or SEAs. As shown in Fig. 5(a), we replaced the spring of the SEA for the vastus muscle by a PAM, and to investigate the effects of a PC, we added a parallel PAM (PPAM) to the combination of EM and serial PAM (SPAM) [see Fig. 5(b)]. This configuration is called electric-pneumatic actuator (EPA) [36]. In Section IV-C, we present the experimental results of controlling the knee joint in quiet standing condition and we show how adjustment of PPAM compliance (through tuning air pressure) can be used for efficient motion control.

In this experiment, we fix the robot trunk orientation by a rigid frame (see [43] for details about this arrangement) while the controlled leg is moving freely (similar to swing leg motion in walking). We also employ the knee actuator to generate a periodic movement at different frequencies. The desired joint position is given by a sinusoidal signal, in which the frequency is increasing linearly from 0.5 to 2 Hz in 5 min. For three different pressure values of SPAM, we investigate the effect of the PC on energy consumption by comparing no PPAM with PAM pressure of 145 and 170 kPa. The integrated square of electric current I in the period of the sinusoidal signal T as given in the following was used as a measure of energy consumption while the movement patterns are kept similar:

$$E = \int_T I^2 dt. \tag{35}$$

As the voltage is similar for all cases, the current can be used to define a measure (E) for energy consumption. It is shown that using an appropriate compliant element result in reducing energy consumption for doing a specific periodic movement. Such an adjustable compliant element can be used in our proposed HPC controller to increase both robustness and efficiency.

IV. RESULTS

A. Simulations: Acrobot Model

As described in Section III-E, the nominal model is walking on flat surface. Then, the maximum slope that a fixed HZD controller can stabilize the walker on (without knowing the slope) is 5°. Here, we present robustness improvement with increasing compliance structure complexity.

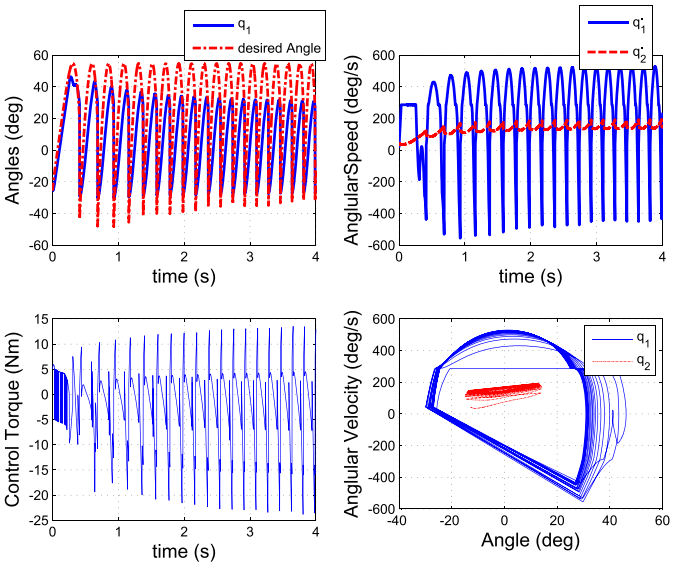

Fig. 3. Specifications of walking on slope 20° with the nonlinear damper $B_d = 2$, $d = 5$ and the nonlinear spring $K_s = 13$, $s = 0.75$.

1) Linear Damper: When linear spring does not improve the motion regarding our target, the first choice is a linear damper. The highest slope that is stabilizable with addition of a linear damper is 7° when $B_d = 0.2$. Compared with the rigid robot, it is qualified to make a periodic walking which satisfies the stability conditions on slightly steeper terrains. Larger coefficients disturb the motion on the flat surface and result in insufficient energy to finish steps successfully.

2) Linear Damper and Linear Spring: When the spring is added to the robot, the allowable range for damper coefficient raises. With $K_s = 13$ and $B_d = 1$, the robot can move stably on slopes between 0° and 10°. Insertion of linear damper and spring does not perturb the limit cycles and the smoothness is preserved. In addition, stable walking with higher speeds is attainable with more energy consumption.

3) Nonlinear Damper: A considerable robustness improvement is gained using a nonlinear damper. One of the most significant advantages of using the nonlinearity is preserving the quality of the motion on the flat surface as much as possible. The nonlinear damper promotes the robot walking robustness to be stable at 17° slope without considerable influence on walking performance on the flat surface.

4) Nonlinear Damper and Nonlinear Spring: The last type of compliance is the combination of a nonlinear damper and a nonlinear spring. This is the most complex mechanism with the best performance. Utilizing this passive structure, the controller qualifies to make a stable walking on slopes up to 20°, as shown in Fig. 3. In the figure, it is observed that after converging to the limit cycle, the steps will be very short and fast. Indeed, it does not yield uncontrollable angular velocities which may result in slippage or falling down. Despite existence of nonsmooth trajectories in phase plane at the beginning of the motion, the limit cycle is almost smooth that means less impacts and losses after convergence to the periodic solution (see Fig. 3, bottom right). The performance of different mechanisms is compared in Table II. The consumed energy [computed by (17)] increases with respect to the slope elevation. It means that for downward slopes above 7°, significant increase in required energy is observed. These results are similar to the experimental findings in human locomotion [44]. At the maximum slope of 20°, our model predicts a walking speed of about 2.5 m s^{-1}.

TABLE II
WALKING PERFORMANCE USING HZD CONTROLLERS WITH DIFFERENT TYPES OF COMPLIANCES

Damper (B_d, d)	Spring (K_s, s)	Energy	Speed	Distance	Slope
—	—	12.52	1.2	4.35	5°
Lin $(0.2, 0)$	—	12.87	1.37	5.05	7°
Lin $(1, 0)$	Lin $(13, 0)$	18.94	1.87	6.66	10°
Non $(2.1, 5)$	—	21.33	2.15	7.76	17°
Non $(2, 5)$	Non $(13, 0.75)$	27.78	2.46	8.73	20°

The Traveled Distance is Considered for 4 s.

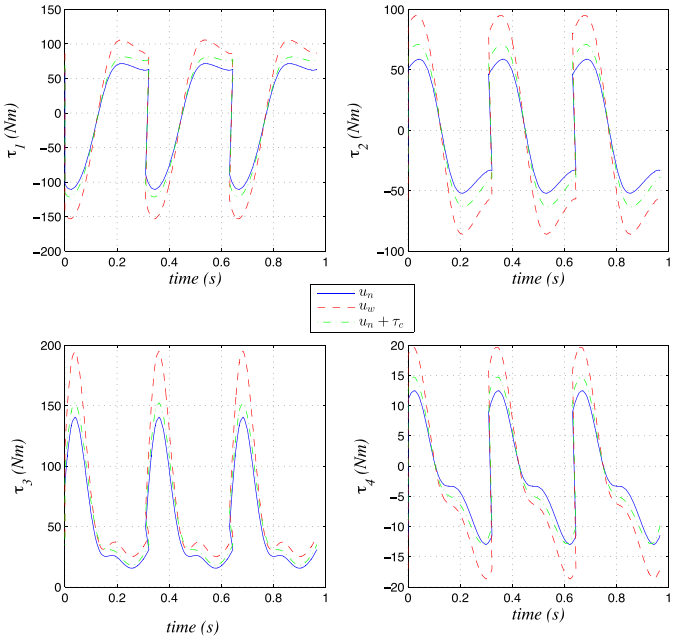

Fig. 4. Comparison between different controllers' actuations on model with 10% uncertainty in segments' lengths. u_n is nominal HZD controller ($L_n = 0.9L$), u_w is HZD control torque knowing the uncertain parameter ($L_w = 1.1L$), and $u_n + \tau_c$ is the control torque of the HPC controller.

B. Walking Robustness With 5-Link Model

In the simulation model of Acrobot, we considered uncertainty in the environment, modeled by unknown ground slope. Here, a second family of modeling uncertainties is addressed by error in body parameters. There is no HZD controller that can stabilize the motion with this uncertainty range. The robot may fall or slip when the controller employs uncertain parameters. To solve this problem, an HPC controller is developed in which the compliance structure is constructed by rotational springs with linear force–angle relations. We define the nominal model with the parameter set $L_n = 0.9L$ (resulting in $u_n = u_{min}$), and the worst case by $L_w = 1.1L$ which means $u_w = u_{max}$. Fig. 4 shows the joint torques of the 5-link model explained in Section III-F. It is observed that the addition of compliance

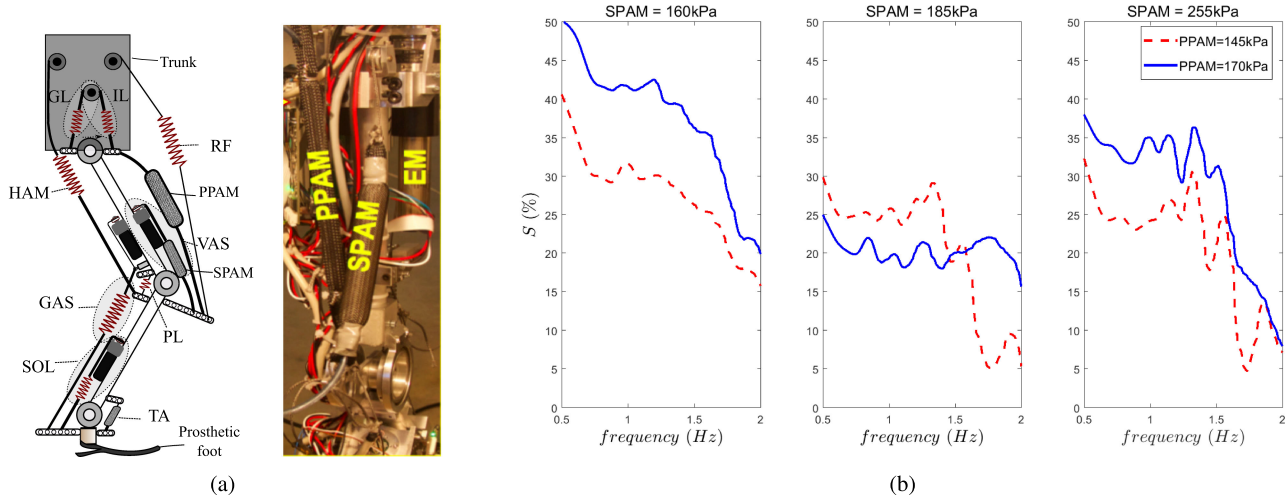

(a) (b)

Fig. 5. (a) Implementation of PC using PAM in BioBiped3 representing the vastus muscle, including one EM, one SPAM, and one PPAM. (b) Experimental results. The desired joint position is a sinusoidal wave with frequency linearly increasing from 0.5 to 2 Hz, over a period of 5 min. The approximation of saved energy (S) compared to no PPAM case is shown for different PAM pressures and oscillations frequencies.

compensates shortage of the control torque in the nominal controller, which is required for stabilization of the worst case model.

C. Hardware Experiments

With the BioBiped3 robot (see Section III-G), effects of PC at different frequencies are shown in Fig. 5(b) for three different pressure values of SPAMs. For each SPAM pressure value, the normalized saved energy (S) is defined by the difference between the consumed energy [calculated by (35)] of that trial (E_p) and the energy of the one from the same group without PPAM (E_0) as follows:

$$S = \frac{E_P - E_0}{E_0}. \tag{36}$$

Positive S values with nonzero PPAM indicate that adding PC reduces energy consumption. In addition, unlike the middle figure, in the left and right figures, the higher PPAM compliance results in a more efficient actuator. Therefore, by introducing a constant parallel compliant structure not only robustness (see Sections IV-A and IV-B), but also energy efficiency can be improved. Therefore, with adjustable PC like the proposed EPA, both efficiency and robustness can be obtained simultaneously for a wide range of gait conditions (e.g., step frequency, speed, and slope).

V. Discussion

In this paper, we studied the role of PC for improving robustness and efficiency in bipedal locomotion. We proposed a design and control approach to benefit from both virtual and physical constraints for robot walking in different walking conditions. In the literature, compliant elements are mostly used for increasing efficiency [22], [45]–[47]. In contrast, here we additionally focused on robustness against uncertainties in body and environmental conditions. With adding parallel elastic elements, stability in larger parameter regions can be achieved without additional need for sensor-based adaptations. Adding PC not only can decrease peak torque and energy consumption [11], [12], but also can reduce the need for further sensory feedback.

One important target in design and control of legged robots is minimizing the efforts required to create walking gaits [48]. Following the mechanical design principles for passive dynamic walking (PDW) [49], bipedal gaits can emerge purely from the natural dynamics of the legs without extra torques. The resulting motions look elegant and humanlike. Similarity between human walking and PDW swing leg movement suggests that humans exploit their natural dynamics with minimized amounts of energy. Although PDWs are not very stable, Collins *et al.* developed a bipedal robots that can walk based on this design concept [32], [50] on a flat surface. To compensate the missing robustness and versatility of PDW, optimal control methods can be utilized [48], [51]. Based on the idea of PDW, we have shown that the mechanical design (e.g. leg compliance and foot curvature) and the matching control are important at the same time for developing an energy efficient robot with humanlike walking [15]. This concept of *control embodiment* [52] is based on high coupling between mechanical design and control [46]. In [15], we have implemented the HZD controller on the springy Acrobot with curved feet (SACF) model as an instance of control embodiment for bipedal walking. Indeed, the mechanical design features (springs, curved feet) and the active components (motors) were acting in series (not like here in parallel). The predicted design advantages (e.g. foot curvature) are in line with findings in human walking [53]. Instead of applying mechanical design modifications (knee and ankle, through leg spring and curved feet, respectively) and the controller (at hip joint by hip actuation) in [15] at different places, in the here presented study we implemented both mechanical and control design at the same joints. As a result, we extend the PDW concept by adding parallel compliant elements. This helped make the system

dynamics robust and efficient, or more humanlike. It means that by adding PC and with adjusting the system dynamics to the desired gait condition, a robust version of PDW paradigm is provided that can be optimally controlled. The robustness is analytically guaranteed as the HZD controller and the PC are designed simultaneously.

The advantages of the parallel elasticity like reducing the required peak power and energy consumption motivate reinforcing SEAs with PEAs [16], [54]–[56]. This additional elements could potentially increase control complexity. To prevent more complication, we presented the HPC control method in a dynamical model with one degree of underactuation. However, this method can be applied to systems with higher degrees of underactuation (e.g., in BioBiped robot). This property is inherited from HZD controller [15], [24] because adding parallel (not serial) passive elements does not change degrees of underactuation.

By defining the function of the parallel compliant elements, we shape the movement solutions by relating them to a submanifold. An appropriate characterization of the compliant elements regarding maximizing robustness can be found using the HZD control approach. We showed that different combinations of linear and nonlinear springs and dampers can increase the robustness against ground slope while nonlinear elements are more effective. This is in line with other studies which successfully implemented nonlinear compliant elements in biped robots [37], [57]. In addition, the significant role of nonlinear compliance has been illustrated in biological systems, e.g., [40], [58].

Recently, different methods were developed for constructing nonlinear compliance [11]. For example, using a specific cam pattern, nonlinear stiffness can be implemented mechanically [59]. In another study, Secer and Saranli suggested three approaches to develop adjustable damping elements [60]. Appropriate implementation of nonlinear compliance could also result in attaining both energy consumption minimization and increasing locomotion speed [61]. Our method is not restricted by the structure of the compliant elements. Therefore, in addition to increasing robustness, reducing energy consumption and improving locomotion speed are expected.

One disadvantage of using PC might be that optimizing it for one particular task avoids achieving efficiency or effectiveness in other tasks. In the biological actuator, an adjustable parallel spring mechanism can be found by the titin filaments that can attach to actin depending the activation dynamics of the muscle (a first mathematical model was provided in [13]). Inspired by this adaptation, our suggested variable compliant elements using pneumatic actuators (described in Section IV-C) could help resolve the aforementioned issue. Therefore, by tuning the air pressure the optimized compliance will provide both efficiency and robustness for a range of motion conditions. Our preliminary results of implementing PAMs as PC (EPA design) on BioBiped3 robot introduces them as appropriate adjustable PC. In the future, we will apply the EPA concept on more joints of the robot for increasing robustness and efficiency in a complete gait.

References

[1] G. A. Pratt and M. M. Williamson, "Series elastic actuators," in *Proc. IEEE/RSJ Int. Conf. Intell. Robots Syst. Human Robot Interact. Cooperative Robots*, 1995, pp. 399–406.

[2] D. W. Robinson, J. E. Pratt, D. J. Paluska, and G. A. Pratt, "Series elastic actuator development for a biomimetic walking robot," in *Proc. IEEE/ASME Int. Conf. Adv. Intell. Mechatronics*, 1999, pp. 561–568.

[3] J. Pratt and B. Krupp, "Design of a bipedal walking robot," in *Proc. SPIE*, vol. 6962, 2008.

[4] K. Radkhah, C. Maufroy, M. Maus, D. Scholz, A. Seyfarth, and O. von Stryk, "Concept and design of the biobiped1 robot for human-like walking and running," *Int. J. Humanoid Robot.*, vol. 8, no. 03, pp. 439–458, 2011.

[5] J. E. Pratt and B. T. Krupp, "Series elastic actuators for legged robots," in *Proc. SPIE*, vol. 5422, 2004, pp. 135–144.

[6] M. Grimmer, M. Eslamy, and A. Seyfarth, "Energetic and peak power advantages of series elastic actuators in an actuated prosthetic leg for walking and running," *Actuators*, vol. 3, no. 1, pp. 1–19, Mar. 2014.

[7] P. V. Komi, "Stretch-shortening cycle," *Strength Power Sport*, vol. 3, pp. 184–202, 2008.

[8] J. W. Hurst, "The role and implementation of compliance in legged locomotion," Ph.D. dissertation, Robot. Inst., Carnegie Mellon Univ., Pittsburgh, PA, USA, 2008.

[9] B. Vanderborght *et al.*, "Variable impedance actuators: A review," *Robot. Auton. Syst.*, vol. 61, no. 12, pp. 1601–1614, 2013.

[10] R. Van Ham, B. Vanderborght, M. Van Damme, B. Verrelst, and D. Lefeber, "MACCEPA, the mechanically adjustable compliance and controllable equilibrium position actuator: Design and implementation in a biped robot," *Robot. Auton. Syst.*, vol. 55, no. 10, pp. 761–768, 2007.

[11] G. Mathijssen, D. Lefeber, and B. Vanderborght, "Variable recruitment of parallel elastic elements: Series–parallel elastic actuators (SPEA) with dephased mutilated gears," *IEEE/ASME Trans. Mechatronics*, vol. 20, no. 2, pp. 594–602, Apr. 2015.

[12] U. Mettin, P. X. La Hera, L. B. Freidovich, and A. S. Shiriaev, "Parallel elastic actuators as a control tool for preplanned trajectories of underactuated mechanical systems," *Int. J. Robot. Res.*, vol. 29, no. 9, pp. 1186–1198, 2010.

[13] C. Rode, T. Siebert, and R. Blickhan, "Titin-induced force enhancement and force depression: A sticky-spring mechanism in muscle contractions?" *J. Theor. Biol.*, vol. 259, no. 2, pp. 350–360, 2009.

[14] P. P. Purslow, "Strain-induced reorientation of an intramuscular connective tissue network: Implications for passive muscle elasticity," *J. Biomechanics*, vol. 22, no. 1, pp. 21–31, 1989.

[15] S. Yazdi-Mirmokhalesouni, M. Sharbafi, M. Yazdanpanah, and M. Nili-Ahmadabadi, "Modeling, control and analysis of a curved feet compliant biped with HZD approach," *Nonlinear Dyn.*, vol. 91, no. 1, pp. 459–473, 2018.

[16] A. S. M. Grimmer and M. Eslamy, "A comparison of parallel and series elastic elements in an actuator for mimicking human ankle joint in walking and running," in *Proc. IEEE Int. Conf. Robot. Autom.*, 2012, pp. 2463–2470.

[17] F. Iida and R. Tedrake, "Minimalistic control of a compass gait robot in rough terrain," in *Proc. IEEE Int. Conf. Robot. Autom.*, 2009, pp. 1985–1990.

[18] F. Iida, Y. Minekawa, J. Rummel, and A. Seyfarth, "Toward a human-like biped robot with compliant legs," *Robot. Auton. Syst.*, vol. 57, no. 2, pp. 137–144, 2009.

[19] E. R. Westervelt, J. W. Grizzle, C. Chevallereau, J. H. Choi, and B. Morris, *Feedback Control Dynamic Bipedal Robot Locomotion*. New York, NY, USA: Taylor & Francis, 2007.

[20] I. Poulakakis, "Stabilizing monopedal robot running: Reduction-by-feedback and compliant hybrid zero dynamics," Ph.D. dissertation, Univ. Michigan, Ann Arbor, MI, USA, 2009.

[21] B. Morris and J. W. Grizzle, "Hybrid invariant manifolds in systems with impulse effects with application to periodic locomotion in bipedal robots," *IEEE Transaction Autom. Control*, vol. 54, no. 8, pp. 1751–1764, Aug. 2009.

[22] K. Sreenath, H.-W. Park, I. Poulakakis, and J. W. Grizzle, "A compliant hybrid zero dynamics controller for stable, efficient and fast bipedal walking on MABEL," *Int. J. Robot. Res.*, vol. 30, no. 9, pp. 1170–1193, 2011.

[23] M. A. Sharbafi, M. J. Yazdanpanah, M. N. Ahmadabadi, and A. Seyfarth, "Parallel compliance design for increasing robustness and efficiency in legged locomotion—theoretical background," *IEEE Trans. Mechatronics*, to be published.
[24] K. A. Hamed and J. W. Grizzle, "Iterative robust stabilization algorithm for periodic orbits of hybrid dynamical systems: Application to bipedal running," *IFAC-PapersOnLine*, vol. 48, no. 27, pp. 161–168, 2015.
[25] E. R. Westervelt, J. Grizzle, and D. E. Koditschek, "Hybrid zero dynamics of planar biped walkers," *IEEE Trans. Autom. Control*, vol. 48, no. 1, pp. 42–56, Jan. 2003.
[26] J. Grizzle, G. Abba, and F. Plestan, "Asymptotically stable walking for biped robots: Analysis via systems with impulse effects," *IEEE Trans. Autom. Control*, vol. 46, no. 1, pp. 51–64, Jan. 2001.
[27] C. Shih, J. W. Grizzle, and C. Chevallereau, "Asymptotically stable walking of a simple underactuated 3D bipedal robot," in *Proc. 33rd Annu. Conf. IEEE Ind. Electronics, Reprint*, 2007, pp. 1404–1409.
[28] J. W. Grizzle, C. Chevallereau, and C. long Shih, "HZD-based control of a five-link underactuated 3D bipedal robot," in *Proc. 47th IEEE Conf. Decision*, 2008, pp. 5206–5213.
[29] H. Khalil, *Nonlinear Systems*. Prentice Hall, Upper Saddle River, NJ, USA, 2002.
[30] A. Isidori, *Nonlinear Control Systems*, 3rd ed. Berlin, Germany: Springer-Verlag, 1995.
[31] J. Choi and J. W. Grizzle, "Feedback control of an underactuated planar bipedal robot with impulsive foot action," *Robotica*, vol. 23, no. 5, 2005, pp. 567–580.
[32] S. Collins, A. Ruina, R. Tedrake, and M. Wisse, "Efficient bipedal robots based on passive-dynamic walkers," *Science*, vol. 307, no. 5712, pp. 1082–1085, 2005.
[33] I. Thorson, M. Svinin, S. Hosoe, F. Asano, and K. Taji, "Design considerations for a variable stiffness actuator in a robot that walks and runs," in *Proc. Robot. Mechatronics Conf.*, 2007, pp. 1–4.
[34] D. Owaki, M. Koyama, S. Yamaguchi, S. Kubo, and A. Ishiguro, "A 2-d passive-dynamic-running biped with elastic elements," *IEEE Trans. Robot.*, vol. 27, no. 1, pp. 156–162, 2011.
[35] H. Geyer, A. Seyfarth, and R. Blickhan, "Compliant leg behaviour explains basic dynamics of walking and running," *Proc. Roy. Soc. B: Biol. Sci.*, vol. 273, 2006, pp. 2861–2867.
[36] M. A. Sharbafi, H. Shin, G. Zhao, K. Hosoda, and A. Seyfarth, "Electric-pneumatic actuator: A new muscle for locomotion," vol. 6, no. 4, p. 30, 2017.
[37] J. D. Karssen and M. Wisse, "Running with improved disturbance rejection by using non-linear leg springs," *Int. J. Robot. Res.*, vol. 30, no. 13, pp. 1585–1595, 2011.
[38] M. A. Sharbafi, M. J. Yazdanpanah, and M. N. Ahmadabadi, "Compliance design in robot structure to increase the robustness," in *Dynamic Walking*, 2011.
[39] M. Garcia, "Stability, scaling, and chaos in passive-dynamic gait models," Ph.D. dissertation, Cornell Univ., Ithaca, NY, USA, 1999.
[40] S. Lipfert, "Kinematic and dynamic similarities between walking and running," Hamburg: Verlag Dr. Kovac, 2010.
[41] D. A. Winter, *BioMechanics and Motor Control Human Movement*, 3rd ed. Hoboken, NJ, USA: Wiley, 2005.
[42] M. A. Sharbafi and A. Seyfarth, "Mimicking human walking with 5-link model using HZD controller," in *Proc. IEEE Int. Conf. Robot. Autom.*, 2015, pp. 6313–6319.
[43] M. A. Sharbafi *et al.*, "A new biarticular actuator design facilitates control of leg function in biobiped3," *Bioinspiration Biomimetics*, vol. 11, no. 4, 2016, Art. no. 046003.
[44] R. Margaria, "Sulla fisiologia e specialmente sul consumo energetico della marcia e della corsa a varie velocita ed inclinazioni del terreno," *Atti Accademia Nazionale dei Lincei*, vol. 7, pp. 299–368, 1938.
[45] J. W. Hurst and A. A. Rizzi, "Series compliance for an efficient running gait," *IEEE Robot. Autom. Mag.*, vol. 15, no. 3, pp. 42–51, Sep. 2008.
[46] P. Gregorio, M. Ahmadi, and M. Buehler, "Design, control, and energetics of an electrically actuated legged robot," *IEEE Trans. Syst., Man, and Cybern., Part B (Cybern.)*, vol. 27, no. 4, pp. 626–634, Aug. 1997.
[47] B. Vanderborght, N. G. Tsagarakis, R. Van Ham, I. Thorson, and D. G. Caldwell, "MACCEPA 2.0: Compliant actuator used for energy efficient hopping robot Chobino1d," *Auton. Robots*, vol. 31, no. 1, p. 55, 2011.
[48] P. Bhounsule, "Control based on passive dynamic walking," in *Bioinspired Legged Locomotion: Models, Concepts, Control and Applications*, M. A. Sharbafi and A. Seyfarth, Eds. Elsevier, Butterworth-Heinemann, 2017, ch. 4.6, pp. 267–291.
[49] T. McGeer *et al.*, "Passive dynamic walking," *Int. J. Robotic Res.*, vol. 9, no. 2, pp. 62–82, 1990.
[50] S. H. Collins, M. Wisse, and A. Ruina, "A three-dimensional passive-dynamic walking robot with two legs and knees," *Int. J. Robot. Res.*, vol. 20, no. 7, pp. 607–615, 2001.
[51] P. A. Bhounsule, J. Cortell, and A. Ruina, "Design and control of ranger: An energy-efficient, dynamic walking robot," in *Proc. Climbing Walking Robots CLAWAR*, Maryland, USA, 2012, pp. 441–448.
[52] R. Pfeifer, M. Lungarella, and F. Iida, "Self-organization, embodiment, and biologically inspired robotics," *Science*, vol. 318, no. 5853, pp. 1088–1093, 2007.
[53] P. G. Adamczyk, S. H. Collins, and A. D. Kuo, "The advantages of a rolling foot in human walking," *J. Exp. Biol.*, vol. 209, no. 20, pp. 3953–3963, 2006.
[54] J. Karssen, "Robotic bipedal running: Increasing disturbance rejection," Ph.D. dissertation, TU Delft, Delft Univ. Tech., Delft, The Netherlands, 2013.
[55] Y. Yesilevskiy, W. Xi, and C. D. Remy, "A comparison of series and parallel elasticity in a monoped hopper," in *Proc. IEEE Int. Conf. Robot. Autom.*, 2015, pp. 1036–1041.
[56] M. Eslamy, M. Grimmer, and A. Seyfarth, "Effects of unidirectional parallel springs on required peak power and energy in powered prosthetic ankles: Comparison between different active actuation concepts," in *Proc. IEEE Int. Conf. Robot. Biomimetics*, 2012, pp. 2406–2412.
[57] S. Cotton, I. Olaru, M. Bellman, T. V. der Ven, J. Godowski, and J. Pratt, "Fastrunner: A fast, efficient and robust bipedal robot, concept and planar simulation," in *Proc. IEEE Int. Conf. Robot. Autom.*, 2012, pp. 2358–2364.
[58] D. F. B. Haeufle, M. Guenther, R. Blickhan, and S. Schmitt, "Proof-of-concept: Model based bionic muscle with hyperbolic force-velocity relation," *Appl. Bionics Biomechanics*, vol. 9, no. 3, pp. 267–274, 2012.
[59] H. J. Bidgoly, A. Parsa, M. J. Yazdanpanah, and M. N. Ahmadabadi, "Benefiting from kinematic redundancy alongside mono- and biarticular parallel compliances for energy efficiency in cyclic tasks," *IEEE Trans. Robot.*, vol. 33, no. 5, pp. 1088–1102, Jun. 2017.
[60] G. Secer and U. Saranli, "Control of planar spring–mass running through virtual tuning of radial leg damping," *IEEE Trans. Robot.*, vol. 34, no. 5, pp. 1370–1383, Oct. 2018.
[61] M. Khoramshahi, H. J. Bidgoly, S. Shafiee, A. Asaei, A. Ijspeert, and M. Nili, "Piecewise linear spine for speedenergy efficiency trade-off in quadruped robots," *Robot. Auton. Syst.*, vol. 61, no. 12, pp. 1350–1359, 2013.

Maziar Ahmad Sharbafi received the B.Sc. degree from the Sharif University of Technology, Tehran, Iran, in 2003, and M.Sc. and Ph.D. degrees from the University of Tehran, Tehran, Iran, in 2006 and 2013, all in control engineering.

He is an Assistant Professor of Electrical and Computer Engineering Department, University of Tehran and a Guest Researcher with the Lauflabor Locomotion Laboratory, TU Darmstadt. His research interests include bioinspired locomotion control based on conceptual and analytic approaches, postural stability, and the application of dynamical systems and nonlinear control to hybrid systems such as legged robots and exoskeletons.

Mohammad Javad Yazdanpanah received the B.Sc. degree from the Isfahan University of Technology, Isfahan, Iran, in 1986; the M.Sc. degree from the University of Tehran, Tehran, Iran, in 1988; and Ph.D. degree from Concordia University, Montreal, QC, Canada, in 1997, respectively, all in electrical engineering.

He is a Professor with the School of Electrical and Computer Engineering, University of Tehran and the Director of the Advanced Control Systems Laboratory. His research interests include analysis and design of nonlinear/optimal/adaptive control systems, robotics, control on networks, and theoretical and practical aspects of neural networks.

Majid Nili Ahmadabadi received the B.S. degree in mechanical engineering from the Sharif University of Technology, Tehran, Iran, in 1990 and the M.Sc. and Ph.D. degrees in information sciences from the Graduate School of Information Science, Tohoku University, Sendai, Japan, in 1994 and 1997, respectively.

He is a Professor with the School of Electrical and Computer Engineering, University of Tehran, Tehran, Iran, where he is a Professor and the Head of Robotics and AI Laboratory. In 1997, he was with the Advanced Robotics Laboratory, Tohoku University. His research interests include cognitive robotics and modeling cognitive systems in addition to control of legged robots.

Prof. Ahmadabadi was a member of the Engineering Board of Iranian National Science Foundation for the period 2005–2011.

Andre Seyfarth received the Vordiplom degree in physics in 1991, the Diploma degree (including B.Sc. and M.Sc.) in physics and biomechanics in 1995, and the Ph.D. degree in biomechanics in 2000 all from Friedrich-Schiller Universität Jena, Jena, Germany.

He is a Professor for Sports Biomechanics with the Department of Human Sciences of TU Darmstadt and the Head of the Lauflabor Locomotion Laboratory. After his studies, he was a DFG Emmy Noether Fellow with the MIT LegLab (Prof. Herr, USA) and the ParaLab, University Hospital Balgrist, Zurich (Prof. Dietz, Switzerland). His research interests include sport science, human and animal biomechanics, and legged robots.

Prof. Seyfarth was the organizer of the Dynamic Walking 2011 conference (Principles and Concepts of Legged Locomotion) and the AMAM 2013 conference (Adaptive Motions in Animals and Machines).